



Universiteit  
Leiden  
The Netherlands

## **A comparison of 3 T and 7 T MRI for the clinical evaluation of uveal melanoma**

Tang, M.C.Y.; Jaarsma-Coes, M.G.; Ferreira, T.A.; Fonk, L.Z.G.; Marinkovic, M.; Luyten, G.P.M.; Beenakker, J.W.M.

### **Citation**

Tang, M. C. Y., Jaarsma-Coes, M. G., Ferreira, T. A., Fonk, L. Z. G., Marinkovic, M., Luyten, G. P. M., & Beenakker, J. W. M. (2021). A comparison of 3 T and 7 T MRI for the clinical evaluation of uveal melanoma. *Journal Of Magnetic Resonance Imaging*, 55(5), 1504-1515. doi:10.1002/jmri.27939





Version: Publisher's Version

License: [Creative Commons CC BY-NC-ND 4.0 license](https://creativecommons.org/licenses/by-nc-nd/4.0/)

Downloaded from: <https://hdl.handle.net/1887/3274126>

**Note:** To cite this publication please use the final published version (if applicable).

# A Comparison of 3 T and 7 T MRI for the Clinical Evaluation of Uveal Melanoma

Michael C.Y. Tang, MD,<sup>1,2\*</sup>  Myriam G. Jaarsma-Coes, MSc,<sup>1,2</sup>  Teresa A. Ferreira, MD,<sup>2</sup>  
Lorna Zwirs - Grech Fonk, MD,<sup>1,2</sup> Marina Marinkovic, MD,<sup>1</sup>  
Gregorius P.M. Luyten, MD, PhD,<sup>1</sup>  and Jan-Willem M. Beenakker, PhD<sup>1,2</sup> 

**Background:** Magnetic resonance imaging (MRI) is increasingly being used in the diagnosis and treatment planning of uveal melanoma (UM), the most common primary intraocular tumor. Initially, 7 T MRI was primarily used, but more recently these techniques have been translated to 3 T, as it is more commonly available.

**Purpose:** Compare the diagnostic performance of 3 T and 7 T MRI of UM.

**Study Type:** Prospective.

**Population:** Twenty-seven UM patients (19% female).

**Field Strength/Sequence:** 3 T: T1- and T2-weighted three-dimensional (3D) spin echo (SE) and multi-slice (MS) SE, 7 T: T1-weighted 3D gradient echo (GE), T2-weighted 3D SE and MS SE, 3 T and 7 T GE dynamic contrast-enhanced. T1 weighted images: acquired before and after Gadolinium (Gd) administration.

**Assessment:** For all sequences, scan and diagnostic quality was quantified using a 5-point Likert scale. Signal intensities on T1 and T2 relative to choroid and eye muscle respectively were assessed as well as the tumor prominence. Finally, the perfusion time-intensity curves (TICs) were classified as plateau, progressive, or wash-out.

**Statistical Tests:** Image quality scores were compared between both field strengths using Wilcoxon signed-rank and McNemar tests. Paired t-tests and Bland–Altman were used for comparing tumor prominences.  $P < 0.05$  was considered statistically significant.

**Results:** Image quality was comparable between 3 T and 7 T, for 3DT1, 3DT2, 3DT1Gd ( $P = 0.86$ ;  $P = 0.34$ ;  $P = 0.78$ , respectively) and measuring tumor dimensions ( $P = 0.40$ ). 2DT1 and 2DT2 image quality were rated better on 3 T compared to 7 T. Most UM had the same relative signal intensities at 3 T and 7 T on T1 (17/21) and T2 (13/17), and 16/18 diagnostic TICs received the same classification. Tumor prominence measurements were similar between field strengths (95% confidence interval:  $-0.37$  mm to  $0.03$  mm,  $P = 0.097$ ).

**Data Conclusion:** Diagnostic performance of the evaluated 3 T protocol proved to be as capable as 7 T, with the addition of 3 T being superior in assessing tumor growth into nearby anatomical structures compared to 7 T.

**Level of Evidence:** 2

**Technical Efficacy:** Stage 3

J. MAGN. RESON. IMAGING 2022;55:1504–1515.

Uveal melanoma (UM) is the most common primary intraocular malignant tumor in adults, with an incidence rate of 6 per million per year.<sup>1</sup> It primarily arises from the choroid (85%), although it can arise from the iris or ciliary body.<sup>2</sup> The main treatment options for UM consist of either eye-preserving therapies, such as proton beam therapy and episcleral brachytherapy, or enucleation, surgical removal of the eye.<sup>2,3</sup> UM patients develop

metastasis regardless of the chosen treatment option in 50% of all cases; the genetic profile of the tumor primarily determines the metastatic risk.<sup>1,4</sup> Gene mutations, and in particular monosomy 3, are known to be associated with increased risk of early-onset metastasis.<sup>2,5</sup> Out of all UM patients, 45% succumb within 15 years, but once metastasized, UM has a poor prognosis with a median survival time of 6.3 months.<sup>6–8</sup>

View this article online at [wileyonlinelibrary.com](http://wileyonlinelibrary.com). DOI: 10.1002/jmri.27939

Received Jul 16, 2021, Accepted for publication Sep 18, 2021.

\*Address reprint requests to: M.C.Y.T., P.O. 9600, 2300 RC Leiden, The Netherlands. E-mail: [m.c.y.tang@lumc.nl](mailto:m.c.y.tang@lumc.nl)

From the <sup>1</sup>Department of Ophthalmology, Leiden University Medical Center, Leiden, The Netherlands; and <sup>2</sup>Department of Radiology, Leiden University Medical Center, Leiden, The Netherlands

Additional supporting information may be found in the online version of this article

This is an open access article under the terms of the Creative Commons Attribution-NonCommercial-NoDerivs License, which permits use and distribution in any medium, provided the original work is properly cited, the use is non-commercial and no modifications or adaptations are made.

Diagnosis, treatment planning, and follow-up are conventionally performed using a combination of optical imaging techniques and ultrasound.<sup>9</sup> Funduscopy evaluation is generally the primary means of detecting UM and the optical characteristics of the lesion provide an important first indication of the type of lesion.<sup>10,11</sup> For example, the funduscopy presence of lipofuscin is often associated with UM.<sup>12</sup> Additionally, ultrasound imaging is used to assess the lesion's internal reflectivity, an important aid in the differential diagnosis, and to measure its dimensions, which determine to a great extent the optimal treatment modality.<sup>9,13</sup>

In the last decade, magnetic resonance imaging (MRI) has become a valuable imaging tool for UM. In the past, its diagnostic value was limited due to the low image resolution and eye-motion artifacts.<sup>14,15</sup> Advances in ocular MRI, such as dedicated eye-coils and eye-specific acquisition strategies, have resolved these limitations, improving the care for UM patients.<sup>16,17</sup> For instance, the acquisition of three-dimensional (3D) images with MRI as opposed to conventional two-dimensional (2D) ultrasound, provides potentially more accurate measurements for treatment planning.<sup>18,19</sup> In addition, functional scans such as perfusion-weighted imaging (PWI) and diffusion-weighted imaging (DWI) can assist the clinical diagnosis and follow-up in UM patients.<sup>16,20–22</sup>

The first developments of these high-resolution ocular MRI technologies were performed at 7 T, where the high

field strength enabled an increased signal-to-noise ratio (SNR) without an increase in acquisition time.<sup>15,23,24</sup> Furthermore, these research-oriented 7 T MRI-scanners provided the platform needed to develop new acquisition strategies to resolve eye-specific challenges, such as eye-motion and an inhomogeneous magnetic field present in the orbit.<sup>15,16,23,25</sup> On 7 T, different clinical applications of ocular MRI for UM emerged; eg, the 3D visualization of the tumor extent had a direct implication on the chosen therapy in a group of UM patients where there were doubts on the conventional ultrasound measurements, enabling eye-preserving therapy in 2 of the 10 included patients.<sup>18</sup> In more recent years, these techniques have been translated to 3 T, as the higher availability would make ocular MRI more accessible to regular clinical care.<sup>26</sup> Initial studies showed the technical feasibility of 3 T in UM, however, both eye-motion and susceptibility-related artifacts proved to be challenging.<sup>14,20</sup>

In this study, we aimed to compare the diagnostic performance of 3 T and 7 T MRI for UM in terms of image quality, radiological characteristics, and tumor dimension measurements.

## Materials and Methods

This single-center prospective cohort study was carried out according to the Code of Ethics of the World Medical Association (Declaration of Helsinki) for experiments involving humans and was approved by

**TABLE 1. Sequence Parameters at 3 T and 7 T**

Sequence Name	Field Strength (T)	Voxel Size (mm <sup>3</sup> )	Sequence	TR (msec)/TE (msec)	Additional Parameters	Scan Time (Minutes:Seconds)
3D						
3DT1 SPIR	3	1.0 × 1.0 × 1.0	SE	350/9.4		3:23
	7	0.4 × 0.4 × 0.9	GE	3.4/6.7	Inversion time: 1280 msec	3:00
3DT2 SPIR	3	0.8 × 0.8 × 0.8	SE	2500/293		3:35
	7	0.6 × 0.6 × 0.6	SE	2500/203		2:25
2D						
MST1 SPIR	3	0.5 × 0.5 × 2.0	SE	718/8		1:16
	7	0.4 × 0.4 × 2.0	SE	745/7.5		1:33
MST2 SPIR	3	0.4 × 0.4 × 2.0	SE	1331/90		1:25
	7	0.45 × 0.45 × 2.0	SE	3000/61		1:18
Dynamic						
DCE	3	1.3 × 1.5 × 1.5	GE	4.5/2.3	2.0 seconds/dynamic	4:20
	7	1.3 × 1.3 × 1.3	GE	3.1/1.8	2.7 seconds/dynamic	3:56

3D = three-dimensional; 2D = two-dimensional; SPIR = spectral presaturation with inversion recovery; MS = multi-slice; DCE = dynamic contrast-enhanced; SE = spin echo; GE = gradient echo; TR = repetition time; TE = echo time.

the local Ethics Committee (CCMO NL57130.058.16). Written informed consent was obtained from all participants of the study. The diagnosis of UM was performed by an ocular oncologist, based on fundus photography, ultrasound, and fluorescein angiography. Tumors were classified according to the American Joint Committee on Cancer (AJCC) 8th edition, based on the clinical ultrasound measurements which were obtained by an ocular oncologist with at least 10 years of experience. Patients were invited to participate in the study following clinical diagnosis.

### Imaging Protocol and MRI Setup

Participants were scanned with a 3-T Ingenia (Philips Healthcare, Best, the Netherlands) and a 7-T Achieva (Philips Healthcare) MRI using the setup and protocols as described earlier by respectively Ferreira et al<sup>26</sup> and Beenakker et al.<sup>23</sup> The main characteristics of the setup and the differences between both field strengths are described below. At both field strengths, the images were acquired with a local receive coil, a 4.7-cm loop coil (Philips) at 3 T, and a 4.5-cm × 3.5-cm home-build coil at 7 T.<sup>23,26</sup> The affected eye was covered with a wet gauze to reduce susceptibility artifacts.<sup>27</sup> During the exam, 0.1 mmol/kg gadoterate meglumine (Dotarem®) was administered with a power injector at 3 T, while it was administered

manually at 7 T. To mitigate eye-motion, a cued blinking protocol was used for the majority of the 7 T scans, where the patient was instructed to focus on a fixation target during the scans. The fixation target was a cross projected on a screen placed at the back entrance of the magnet bore, at approximately 1.3 m distance from the subjects' head. A small mirror, incorporated in the receive coil's housing enabled the subject to see the cross. The scan was automatically paused every 3 seconds and the patient was visually instructed to blink.<sup>23</sup> At 3 T, the patients were simply asked to keep their eyes closed and to try to minimize eye-motion as much as possible.

The MRI exams were performed on separate days, to ensure no contrast agent was present from the previous scan. Since UM patients are generally treated soon after diagnosis, no randomization was performed on which field strength was performed first, but rather the field strength of the first scan was dependent on the availability of the MRI scanner.

The scan protocol, shown in Table 1, consisted of multiple sequences which were designed to answer specific clinical questions.<sup>26</sup> At 3 T, T1 and T2 weighted 3D spin echo (SE) sequences were used to assess the tumor dimensions in 3D. At 7 T, T1 weighted gradient echo (GE) and T2 weighted SE sequences were used for the same purpose. At both 3 T and 7 T SE sequences were used for multi-slice (MS) 2D acquisitions. These sequences had an increased in-plane resolution compared to 3D sequences to assess the origin of lesion and to detect potential involvement of adjacent anatomical structures, such as the optic nerve or ciliary body. All T1 weighted sequences were acquired before and after Gadolinium (Gd) administration. The acquisition times of the different scans were chosen to be approximately similar on both field strengths, 3 minutes for the 3D sequences and 1.5 minutes for the 2D sequences. In addition, both field strengths acquired GE dynamic contrast-enhanced (DCE) scans for PWI, which can aid in the differential diagnosis of intra-ocular lesions.<sup>20,21</sup>

### Evaluation

All assessments related to image quality, signal intensities, tumor dimensions, and involvement of nearby structures were performed in Sectra IDS7 (Sectra AB, Linköping, Sweden, version 21.2).

The observers were not masked at which field strength the images were acquired, as the distinct differences in image appearance of the MR-images acquired at 7 T and 3 T, eg, different field-of-view and images contrast, made it immediately apparent on which field strength the image was acquired. The exams were, however, evaluated in separate sessions, and the observers were blinded to the interpretation of the other field strength images and to the clinical ophthalmic data (such as that from ultrasound images).

The evaluation criteria for image quality and signal intensities were set by MJ, TGF, and JWB, a medical technician with 2 years of experience in ocular MRI, a neuroradiologist, and an ophthalmic MR-scientist, both with at least 9 years of experience in ocular MRI. The criteria were based on a different cohort of patients and these matched those used in an earlier study.<sup>26</sup> The image quality and signal intensities were scored by three of either JWB, MJ, MT, or TGF. In case of doubt or disagreement, JWB, MJ, and TGF jointly evaluated the images, and the final score was based on consensus. Likewise, JWB, TGF, and MJ scored all MS images for the presence or absence of the following: signs of involvement of nearby

**TABLE 2. Patient Characteristics**

Characteristic	Scanned Patients (N = 25)
Sex-no. (%)	
Male	21 (84%)
Age (years)	
Median (interquartile range)	66 (59–73)
Eye-no. (%)	
OS	8 (32%)
OD	17 (68%)
AJCC classification <sup>a</sup> (%)	
T1	4 (16%)
T2	7 (28%)
T3	8 (32%)
T4	4 (16%)
Iris	2 (8%)
Treatment received (%)	
Brachytherapy	15 (60%)
Proton beam therapy	4 (16%)
Enucleation	6 (24%)

<sup>a</sup>The American Joint Committee of Cancer (AJCC) 8th edition classification was based on ultrasound measurements. OS = left eye; OD = right eye.

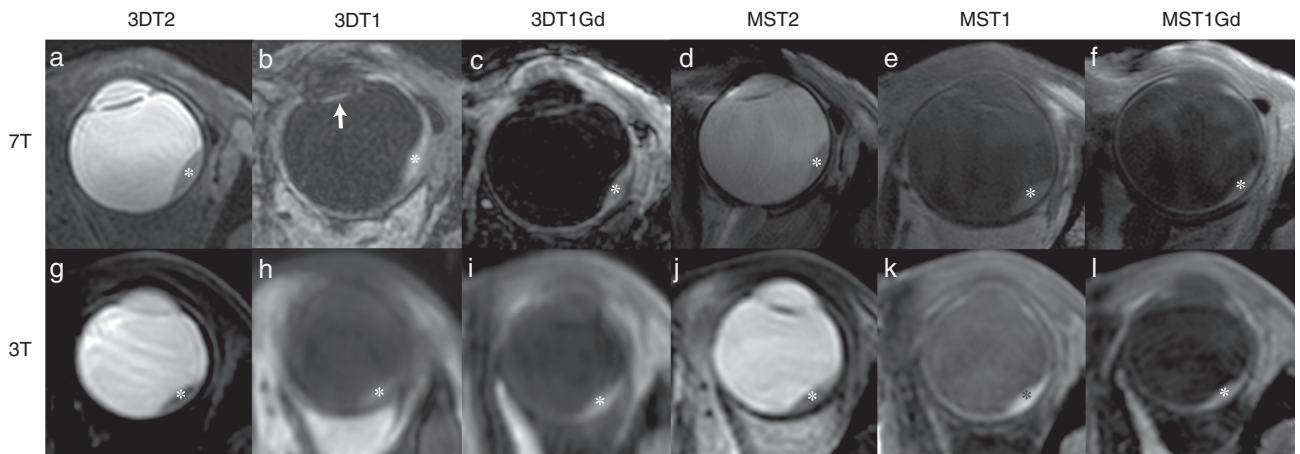


**FIGURE 1:** A side-by-side comparison of the scans of one patient with uveal melanoma (UM) (asterisk) on 7 T (a–f) and 3 T (g–l). (a, g) 3DT2 SPIR. (b, h) 3DT1. Note the intraocular lens after cataract surgery (arrow). (c, i) Contrast-enhanced 3DT1 SPIR (d) MST2 SPIR (j) MST2 without fat suppression. (e, k) MST1 SPIR. (f) Contrast-enhanced MST1 without fat suppression. (l) Contrast-enhanced MST1 SPIR.

structures, tumor heterogeneity, extra scleral extension, and retinal detachment (RD). Tumor heterogeneity was defined by the presence of signal intensity differences within the tumor, which could be observed on either 2D or 3D scans.

MR image quality was rated using a 5-point Likert scale.<sup>26</sup> Images with a score of 1 were deemed undiagnostic (eg, severe artifacts or artifacts in the area of interest), while images with a score of 5 were of the highest quality (eg, no artifacts or minimal artifacts outside of the area of interest). A score of 3 was the threshold for an image to be diagnostic, which, however, did not exclude the presence of artifacts or noise in the image.<sup>26</sup> The overall image quality was rated for all anatomical sequences. Additionally, the 3D scans were also rated for the quality to assess the tumor dimensions, while

the ability to determine the tumor limits was rated on the 2D scans. Artifacts found during the scoring process were noted, in addition to the location and the cause for the artifact, eg, ghosting due to eye movement.

On T1 weighted images, the signal intensity of the UM was compared to the signal intensity of the choroid, as this provided a better reference than the vitreous, and classified as hyper-, iso-, or hypointense.<sup>26</sup> Similarly, on T2 weighted images, the signal intensity was compared to the most adjacent extra-ocular muscle.

The tumor prominence was determined using multi-planar reconstructions (MPR) on the isotropic 3D scans. The measurements were taken on the 3D sequence on which the limits of both the tumor and the sclera were visualized best, generally the contrast-enhanced T1.

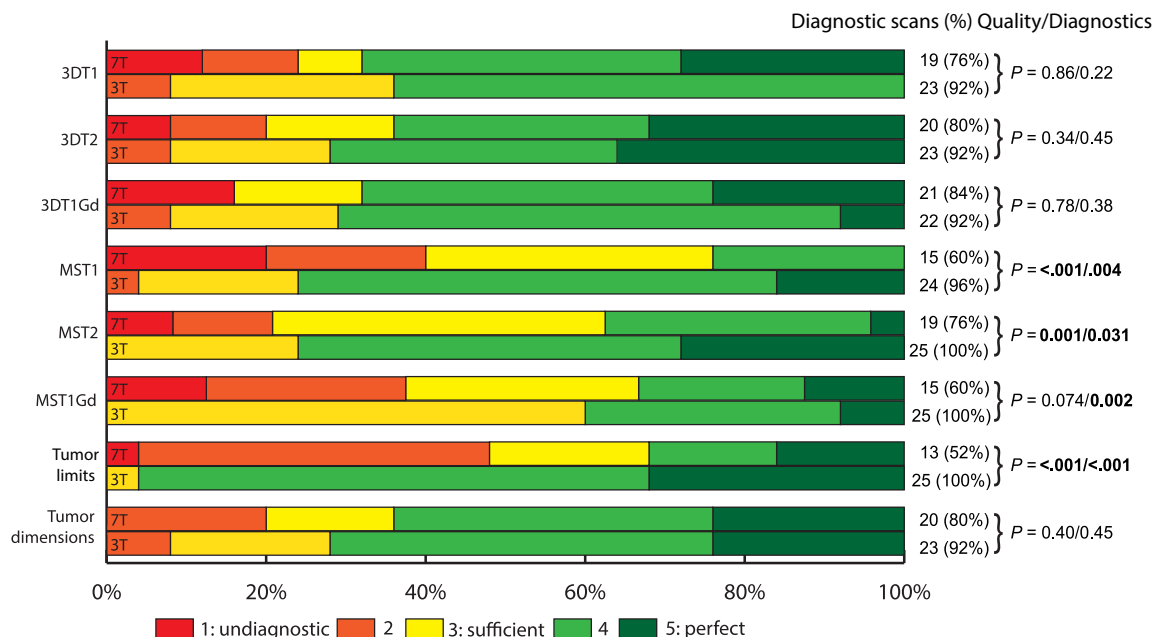


**FIGURE 2:** (Left) Overview of the image and diagnostic quality scores for each of the scan sequences on 3 T and 7 T. (Right) The cutoff for a diagnostic image quality was 3. The difference in quality score between 7 T and 3 T was tested using the Wilcoxon signed-rank test, while the McNemar tested for the difference in diagnostic scans. The majority of the scans on both 3 T and 7 T were diagnostic (95% vs. 73% respectively). For the 3D sequences the image qualities were not significantly different ( $P > 0.3$ ), while the 2D sequences were rated better on 3 T ( $P < 0.001$ ) with the exception of the 2D T1 after contrast ( $P = 0.074$ ).

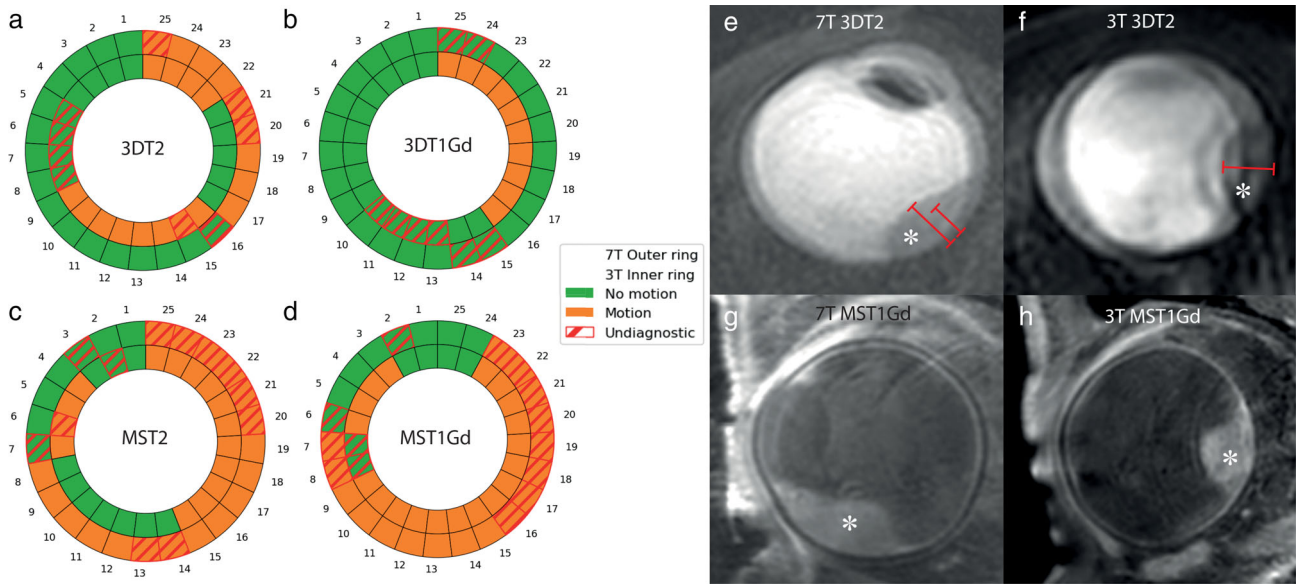


**FIGURE 3:** (a–d) Presence of motion artifacts on a representative set of sequences per patient, with 7 T on the outer ring and 3 T on the inner ring. Red markings indicate an undiagnostic image. Examples of differences in the impact of these artifacts on the diagnostic quality of the image are shown in (e–h). (e, f) Due to motion, the uveal melanoma (UM) (asterisk) can appear double on the image. In one exam (e) this resulted in two different potential prominence measurements (6.2 mm and 5.0 mm), while on another exam (f) an accurate measurement could still be made. (g) 7 T MST1Gd and (h) 3 T MST1Gd image of diagnostic quality with ghosting.

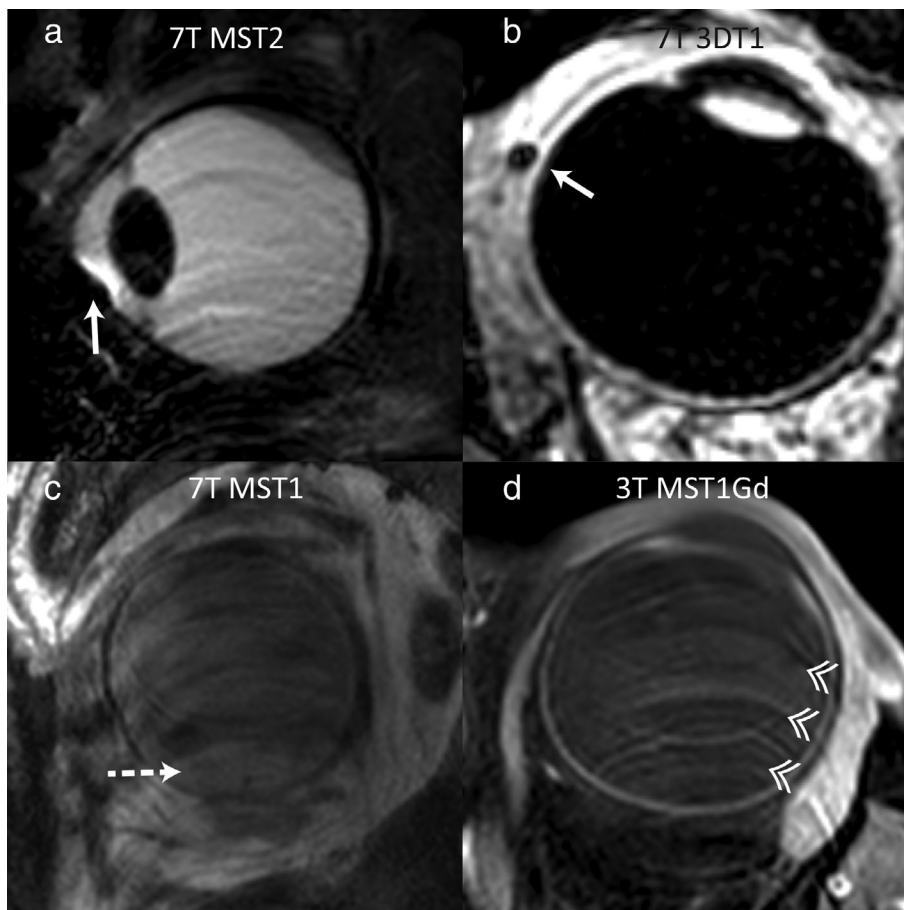


**FIGURE 4:** Magnetic resonance imaging (MRI) artifacts on 7 T (a–c) and 3 T (d). (a, b) On 7 T, susceptibility artifacts were commonly observed (arrows) (rated diagnostic, 3/5 Likert scale). (c, d) On both field strengths, motion artifacts were commonly observed, causing ghosting on the images (arrowheads). In these examples of two different patients, the artifacts rendered the 7 T images undiagnostic (1/5 Likert scale), while the 3 T was still scored as diagnostic (3/5 Likert scale). Note that the 7 T image (c) seemingly shows a UM lesion (dashed arrow) at the bottom of the eye, while this is in fact caused by the ghosting artifact.

Prominence was defined as the tumor thickness, including the sclera, to match those of the clinical ultrasound measurements used for dose calculations for episcleral brachytherapy.<sup>28</sup> JWB in conjunction with MT, an MD with 1 year of experience in ocular MRI, measured the tumor prominence for all patients.

The PWI data were evaluated using MATLAB (version 2019b, The MathWorks, Inc., Natick, MA, USA) by MJ. The tumor was delineated semi-automatically in 3D by MJ using MeVisLab (version 3.0.2, MeVis Medical Solutions AG, Bremen, Germany) and the reliability of the resulting time-intensity curve (TIC) was subsequently scored by JWB, MJ, and MT, as no motion visible, motion while still diagnostic or undiagnostic due to motion. The classification for “motion while still diagnostic” was given to TICs with temporary changes in signal intensity, but these spikes did not hinder a visual assessment of the TIC. In cases of disagreement, JWB, MJ, and MT jointly evaluated the TIC to reach a reliability score based on consensus. All diagnostic TICs were subsequently classified as either a progressive, washout, or plateau curve type as described by Yuan et al.,<sup>29</sup> with the slight modification that the TICs were classified at 2 minutes after inflow instead of 5 minutes, as it is less susceptible to motion.

### Statistical Analysis

All statistical analyses were performed using IBM SPSS Statistics (version 25.0.0.2, IBM, Armonk, NY, USA). A Bland–Altman was used to compare MRI tumor prominence measurements between

field strengths. Wilcoxon signed-rank tests were used for quality assessments using a Likert scale and assessments of TIC motion. The McNemar test was used for paired dichotomous nominal data. Paired *t*-tests were used for comparing mean differences between paired measurements. *P* values equal to or below 0.05 were considered significant.

### Results

A total of 27 UM patients were enrolled in the study. Two patients were excluded after only finishing a 7-T scan: one patient choose to withdraw from the study after the first scan and the second patient was excluded due to a medical complication, unrelated to the UM or first MRI scan, between the two MRIs.

Median age at the time of diagnosis for all remaining patients was 66 years (range 24–90). Four of 25 patients were female. In 17/25 patients the UM was in the right eye. The majority (60%) of patients received brachytherapy treatment and all tumor classes, according to the American Joint Committee on Cancer (AJCC) 8th edition classification, were present in the cohort as can be seen in Table 2. The average UM prominence, based on ultrasound, was 6.4 mm (range 2.9–12.3).

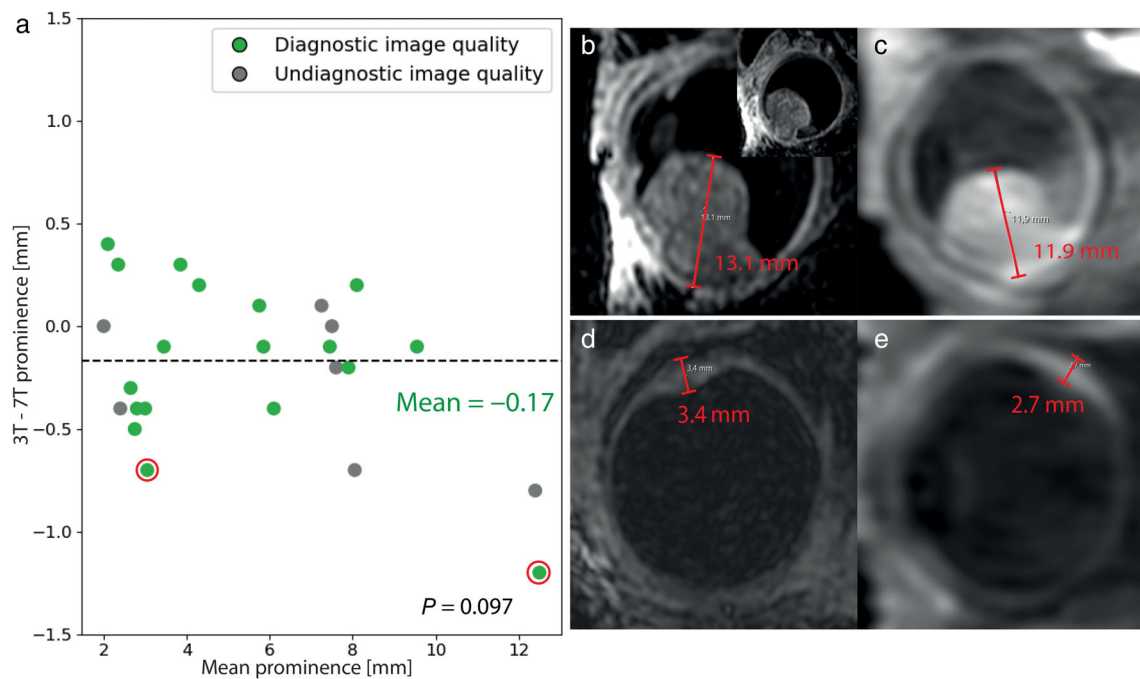


**FIGURE 5:** (a) Bland–Altman plot comparing the uveal melanoma (UM) prominence measurements made using multi-planar reconstructions (MPR) of the 3D MR-images on 7 T and 3 T, showing no significant differences in the diagnostic cases ( $P = 0.097$ ). Patients in whom the scan quality to measure tumor dimensions were rated as sufficient or higher on both modalities are depicted in green, patients in whom one or both scans were graded undiagnostic in gray. No significant prominence measurement differences were present when taking into account the undiagnostic cases ( $P = 0.243$ ). The mean difference in prominence measurements for the diagnostic scans was  $-0.17$  mm, and  $-0.20$  mm when the undiagnostic scans were included as well. The two patients with diagnostic scans and a larger than 0.5 mm prominence difference are shown in (b–e). (b, c) Patient with a large mushroom-shaped UM (inset: perpendicular reconstruction), where due to the complex shape, the prominence was measured in a different direction between 3 T and 7 T. In addition, the outer scleral limits could not well be determined on both field strengths. (d, e) A small UM, which in retrospect, received a prominence measurement that was too small on 3 T, due to a blurred inner limit at 3 T, which was more clearly distinguishable at 7 T.

The 7 T scan was performed first in 60% of the patients. The average time in between 7 T and 3 T exams was 4 days (range 1–16). One patient did not finish the last part of the 3 T exam, due to which the contrast-enhanced 3D T1 weighted image was not acquired. This patient was excluded from the analysis of the 3DT1Gd scans. As a result, for all analyses, 25 patients with matching 7 T and 3 T exams were analyzed, with the exception of the 3 T 3DT1Gd analysis, which was performed for 24 patients.

**Image Quality**

Although the majority of 3 T and 7 T images met diagnostic quality standards in our assessments, as can be seen in (Fig. 1), noticeable differences were apparent after evaluating the image quality scores (Fig. 2).

On average, the 3DT1, 3DT2, and 3DT1Gd scans were rated similar in overall image quality between 3 T and 7 T, ( $P = 0.86$ ;  $P = 0.34$ ,  $P = 0.78$ , respectively). At 7 T, 3D scans rated a perfect score of 5 on the Likert scale in 28% of scans as compared to 15% of scans at 3 T. However, 12%

of 7 T 3D scans also received the lowest score on the Likert scale, while none were given to any 3D scans at 3 T. As a result, no significant differences were found in overall image quality for 3D scans at either field strength. The 3DT1, 3DT2, and 3DT1gd scans were also rated similar in terms of reacting diagnostic image quality, a score of 3 on the Likert scale ( $P = 0.22$ ;  $P = 0.45$ ;  $P = 0.38$ , respectively).

The evaluation of how well the 3D scans could be used to assess the 3D tumor dimension, received a similar result, with 94% of the 3 T and 80% of the 7 T being rated of diagnostic quality ( $P = 0.45$ ).

In general, 3 T 2DT1, 2DT2, and 2DT1Gd scans, used to assess the tumor limits, were rated higher in overall image quality than their 7 T equivalents. At 3 T, 2D scans achieved a perfect score of 5 on the Likert scale in 17% of scans as opposed to 7% at 7 T. Furthermore, only 1% of 3 T 2D scans received a score of less than 3 as compared to 31% for 7 T 2D scans, which would result in the scan as being undiagnostic. As a result, the different 3 T 2D sequences rated significantly higher in overall image quality score

**TABLE 3. Appearance of Uveal Melanoma on 3 T and 7 T MR-Images**

<b>A. Relative signal intensity on T1</b>				
<b>7 T</b>	<b>Hyperintense</b>	<b>Isointense</b>	<b>Hypointense</b>	<b>Total</b>
3 T				
Hyperintense	10	1	0	11 (52%)
Isointense	2	6	0	8 (38%)
Hypointense	0	1	1	2 (10%)
Total	12 (57%)	8 (38%)	1 (5%)	Same intensity: 17/21 (81%)
<b>B. Relative signal intensity on T2</b>				
<b>7 T</b>	<b>Hyperintense</b>	<b>Isointense</b>	<b>Hypointense</b>	<b>Total</b>
3 T				
Hyperintense	13	0	0	13 (81%)
Isointense	3	0	0	3 (19%)
Hypointense	0	0	0	0 (0%)
Total	16 (100%)	0 (0%)	0 (0%)	Same intensity: 13/16 (81%)

The relative signal intensities (SIs) on T1 compared to choroid were similar in 81% of the UM patients between modalities. In addition, on T2 the relative SI compared to ocular muscles were also similar in 81% of the patients.



compared to 7 T, with the exception of the 7 T 2D scan after contrast ( $P = 0.074$ , Fig. 2).

Two-dimensional scans were rated diagnostic after receiving a Likert score of at least 3, which meant that they were sufficient for clinical diagnostic use. At 3 T, 99% of 2D scans were rated diagnostic. By comparison, 69% of the 7 T 2D images were given a similar score of 3 and higher, which left 1/3 of the 7 T images of undiagnostic image quality. The result was, all 3 T 2D sequences rated significantly better than 7 T in terms of reacting diagnostic quality.

As a result, 3 T scans, with the exception of the 2DT1Gd, were rated significantly better than the 7 T scans in terms of delineating the tumor limits. Additionally, the severity of the artifacts on 7 T more often hindered a detailed evaluation of the tumor limits, while on 3 T these evaluations were generally still possible in the presence of artifacts (Fig. 3g,h). This was made evident as 32% of 7 T 2D images, which contained artifacts, scored lower than 3 points on image quality as opposed to 2% for 3 T 2D scans which contained artifacts.

A wide array of artifacts were seen in both 3 T and 7 T images (Fig. 4). In 73% of the 3 T and 89% of the

7 T scans, artifacts were observed. On 3 T, the predominant artifact was ghosting due to movement of the eye, which accounted for 59% of the observed artifacts on the 3 T images (Fig. 3). Other observed artifacts included: blurring 11%, fold-over 1%, susceptibility artifacts 5%, and Gibbs ringing 2%. On 7 T images, 46% of the images suffered from ghosting, which accounted for 35% of the 7 T artifacts. On most of the 7 T images, susceptibility artifacts were observed, likely caused by small air bubbles under the eyelid (Fig. 4a), accounting for 41% of 7 T and only 6% of 3 T artifacts. Additionally, in the 7 T scans of 2 patients large signal voids were observed, which were attributed to a susceptibility artifact in the anterior part of the eye of one subject, and a failed coil calibration in the other subject. Overall, however, the presence of these artifacts did not necessarily result in undiagnostic images as the localization, extent and diagnostic impact of artifacts differed from scan to scan (Fig. 3e–h). Overall, 3 T images with motion-related artifacts were more frequently of diagnostic value than 7 T images with similar motion-related artifacts, with 98.5% as compared to 80% of scans being diagnostic, respectively. Furthermore, the susceptibility

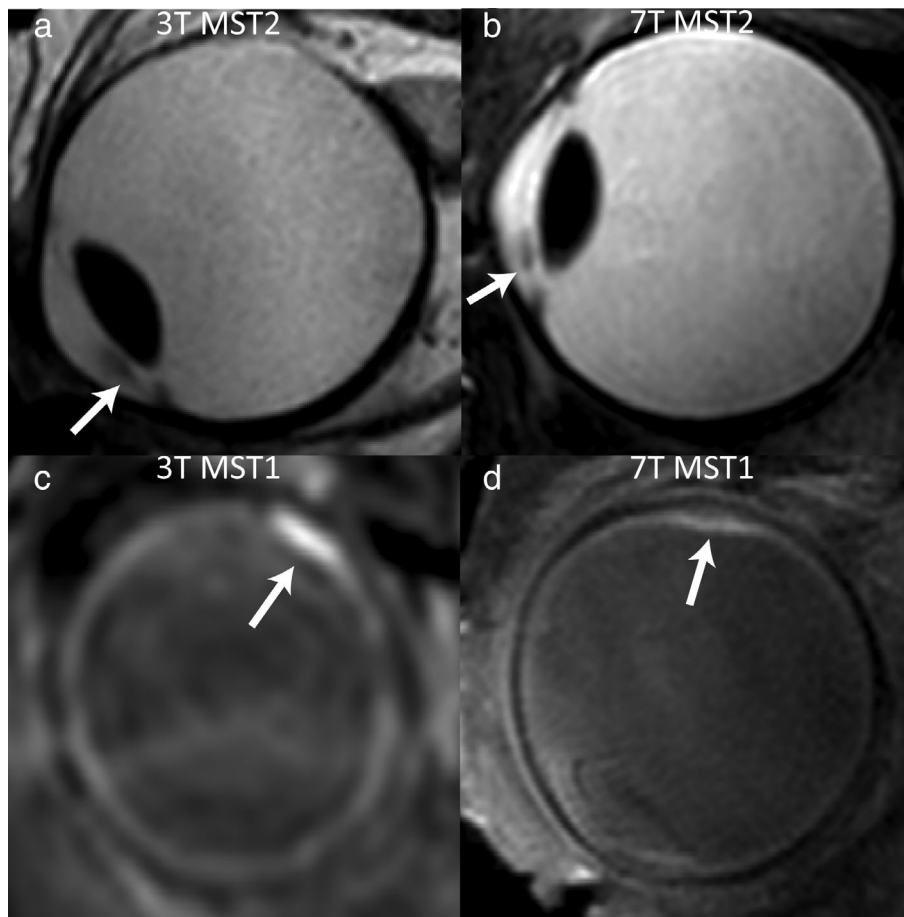


**FIGURE 6:** Side-by-side comparisons of magnetic resonance (MR)-images of a patient with a small uveal melanoma (UM) located in the iris (a/b) and choroid (UM) (c/d) acquired on 7 T (b/d) and 3 T (a/c). UMs are indicated by a white arrow. (a/b) On MST2, an iris melanoma of less than 1 mm in size could be seen on both field strengths, although it was more clearly delimited on 7 T. (c/d) Example of a small UM which was classified as homogeneous on MST1 at 3 T and heterogeneous on MST1 at 7 T.

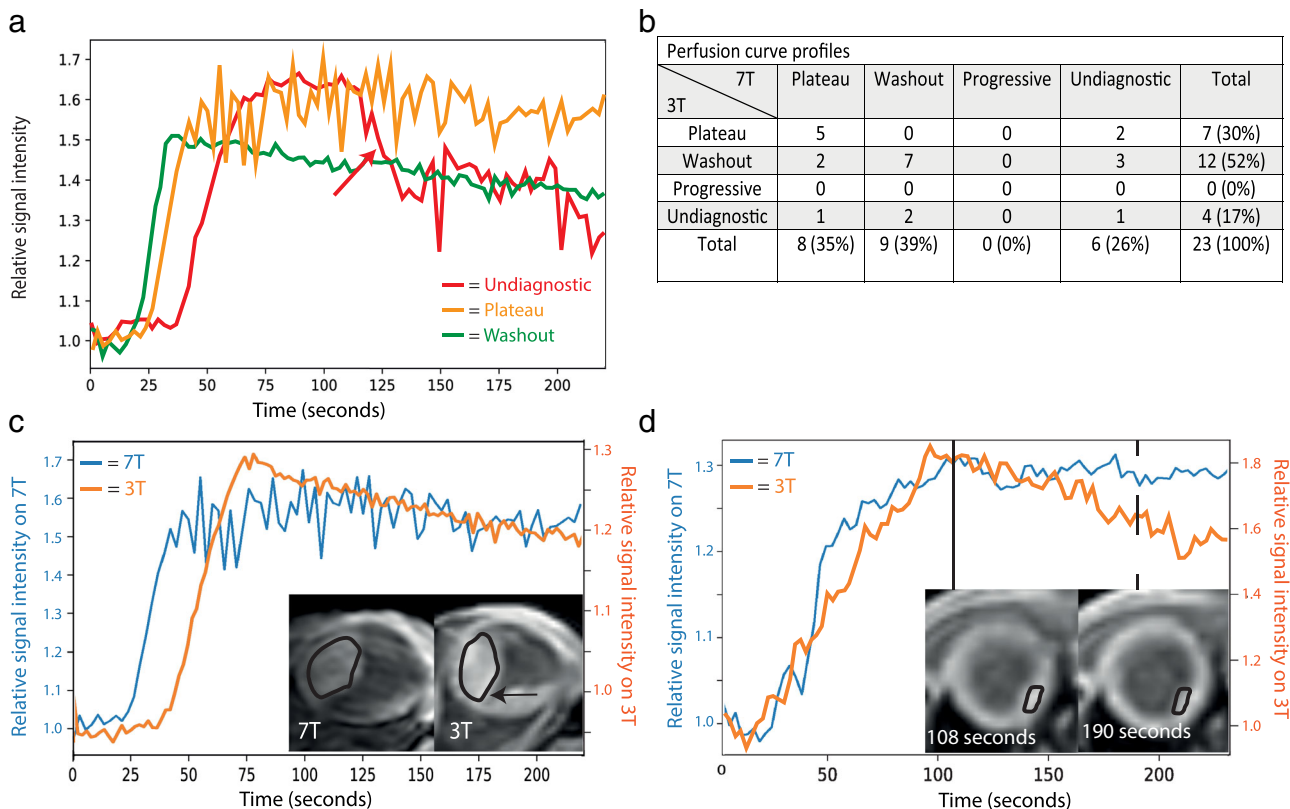


**FIGURE 7:** (a) Three examples of perfusion curve profiles. (Green) A diagnostic washout curve with no motion. (Orange) A plateau type curve profile, which contained motion, but still considered diagnostic. (Red) An undiagnostic time-intensity curve (TIC), as shown by the sudden drop in signal intensity (red arrow), caused by eye motion. (b) Comparison of perfusion curve classifications on 7 T and 3 T, showing the same classification of diagnostic curves for all except two patients, which are shown in (c, d). The difference in TIC was attributed to the erroneous inclusion of retinal hemorrhage on the 3 T analysis (black arrow). (d) The 3 T TIC shows a decrease in relative intensity after 100 s. This was however not the result of a reduction in gadolinium concentration, but due to motion, resulting in an erroneous wash-out classification. The two 3 T images depict this motion and the effect on the drawn region-of-interest.

artifacts found in 7 T were often located outside the area of interest such as below the eyelid and did therefore not interfere with clinical evaluation.

**Tumor Dimensions**

The UM prominence measurements, which can be found in the Supplemental Material, were comparable on both field strengths. Overall, differences in measurements between 7 T and 3 T were less than 0.5 mm (Fig. 5) for the 18/25 scans which were diagnostic on both field strengths. The 3 T measurements were on average 0.17 mm smaller than on 7 T, with an average absolute difference of 0.34 mm, resulting in no significant difference ( $P = 0.097$ ). Moreover, even measurements performed on images with undiagnostic quality differed less than the voxel size, with the 3 T measurements being on average 0.20 mm smaller than 7 T when also the undiagnostic images were included, but not significantly ( $P = 0.243$ ).

**Appearance on MRI**

Generally, UM appeared similar in scans at both field strengths for the majority of patients (Table 3). For example, 81% of

UM had the same relative signal intensity compared to the choroid on T1, while in the remaining patients only a subtle difference in relative signal intensity was observed. For both T1 and T2, the differences were primarily caused by five small UM with a prominence <3 mm. The three other similar-sized lesions appeared hyperintense on T2 at 7 T but isointense at 3 T. For most small lesions the signal intensity could be determined, such as a small iris lesion (Fig. 6a,b), but of one patient an accurate assessment of an iris lesion was not possible on T2.

The UM appeared more frequently heterogeneous on 7 T than 3 T, of which examples can be seen in (Fig. 6c,d). For instance, 41% of 7 T images on T1 were classified as heterogeneous UM as opposed to only 18% on 3 T. Moreover, RD was observed in 56% of the UM patients, with no differences between 3 T and 7 T.

**Perfusion-Weighted Imaging**

On 7 T, more perfusion curves were classified as undiagnostic than on 3 T, with 26% of 7 T perfusion curves classified as undiagnostic due to motion compared to 17% on 3 T (Fig. 7). Furthermore, 44% of the 7 T and 56% of the 3 T

TICs contained motion but were still graded as diagnostic. The remainder of 7 T and 3 T curve profiles were, respectively 30% and 26%, diagnostic without motion.

No significant difference was found between 7 T and 3 T in the pairwise comparison of reliability classifications ( $P = 0.156$ ), nor were there differences between diagnostic and undiagnostic TIC classifications between 7 T and 3 T ( $P = 0.727$ ). Approximately half of the diagnostic curves were classified as plateau (42%) and the other half as washout (58%). All diagnostic curves received the same classification on both field strengths, except two patients who were classified as washout on 3 T and plateau on 7 T.

## Discussion

We showed that, despite the lower field strength, 3 T performed similar or better compared to 7 T in aspects such as image quality, the ability to determine tumor dimensions, and tumor limits.

The appearance of UM on 7 T and 3 T MR images in terms of signal intensities on T1 and T2 was comparable for most patients, although heterogeneity in smaller lesions could be observed on 7 T images, which were often not observed on 3 T images. This discrepancy between both field strengths was primarily observed in smaller sized UM, where the resolution of the 3 T images was apparently not sufficient to detect the inhomogeneity.

However, for current clinical practice, the observation of a heterogeneous tumor does not have any clinical consequences, as the clinical workup is based on the dimensions and localization of UM.<sup>2</sup> Other findings such as RD, commonly accompanying UM, were found consistently well on either modality. On PWI, the vast majority of the UM showed similar characteristics on both field strengths. In the only two cases with a different TIC between the field strengths, this was attributed to factors unrelated to the field strength. Adjacent to one of these UM was a large retinal hemorrhage. On 7 T this hemorrhagic component was not included in the ROI, while it was, erroneously, included on 3 T images, causing the observed difference in TIC. A retrospective evaluation of the 3 T images of the other patient showed a slight shift in gazing direction during the dynamic acquisition, making the small tumor move outside of the ROI, resulting in an erroneous washout classification. Finally, on 7 T more susceptibility artifacts were observed than on 3 T, but since these were generally limited to the anterior part of the eye, these did not have any clinical consequences.

The 3D sequences were used primarily to determine the tumor dimensions, while the ability to determine the tumor dimensions on the MPR was assessed separately. We found both aspects to be comparable between 7 T and 3 T 3D scans. Yet the 7 T 3D scans did produce more perfect rated images compared to 3 T, however, 3 T proved to be more

consistent in producing images of adequate quality for clinical use. Part of this difference can likely be explained by the different acquisition strategy. On 3 T, it was decided that non-blinking protocol would benefit a wider clinical adoption of MRI in UM patients, as compared to modifications and extra equipment required for a cued-blinking protocol. The 7 T, however, did use a cued-blinking approach which was used to mitigate eye-motion. Although, the cued-blinking approach can be a very effective method to prevent eye-motion artifacts, as is shown for example by the 13% of 7 T 3D scans without motion artifacts compared to 41% at 3 T. However, not all patients successfully adhered to this cue-blinking protocol. For these patients, a considerable drop in image quality was observed, as less data can be acquired, due to blinking pauses, resulting in more pronounced artifacts in the case of eye-motion. Despite these differences, however, tumor prominence measurements were highly comparable between field strengths, with a mean difference below 0.2 mm, well below the isotropic voxel size of 3DT1 at 3 T or 7 T (1.0 mm and 0.4 mm, respectively). By comparison, Char et al reported an interobserver variability for clinical ultrasound in UM of 0.6 mm,<sup>30</sup> showing that this small difference between the 3 T and 7 T is less than the interobserver-variation of current clinical reference standard. Furthermore, Ferreira et al recently reported an improved version of both the 3D T1-weighted and T2-weighted sequences on 3 T, with reduced scan times of respectively 76 and 37 seconds, as well as an increased spatial isotropic resolution of 0.8 mm.<sup>31</sup> As the resulting images have an improved depiction of the tumor boundaries, we expect that this new protocol will result in overall better 3D images than the 7 T protocol.

The 2D scans were generally preferred to assess the involvement of adjacent structures due to their higher in-plane resolution and overall image quality. In this study, in contrast to the 3D scans, the 2D scans rated significantly better on 3 T than on 7 T in terms of image quality and tumor delineation. These differences appeared to be primarily attributed to the sharper tissue boundaries on 3 T, especially between the UM and sclera, which were often difficult to see on T1 and contrast-enhanced T1 7T scans. On the T2 weighted scans, however, the sclera could generally be well differentiated on both the 7 T and 3 T images. Given the increased signal intensity at 7 T, a better delineation at 7 T could be expected, as this was also observed in different studies of other anatomies. Steensma et al, eg, showed that for imaging the prostate a higher SNR could be achieved using 7 T.<sup>32</sup> Similarly, Maruyama et al described a superior delineation of anatomical brain structures on 7 T, while Hartevelde et al showed that small lesions in the arterial vessel walls could be visualized much better on 7 T than on 3 T.<sup>33,34</sup> However, unlike the aforementioned studies with up to 20 minutes per sequence, imaging the eye requires short acquisition times to limit eye-motion related artifacts. As a

result, the image resolution was limited by the number of k-space lines that could be acquired within 4 minutes.<sup>18,23</sup> Additionally, due to specific absorption rate (SAR) limitations, the 7 T scans could not use 180° refocusing pulses, which, given the susceptibility differences of the sclera and orbital fat, resulted in a less sharply defined sclera on the 7 T images.<sup>35</sup> This reduction in image quality can have direct clinical implications, as it hinders accurate assessment of the involvement of the surrounding tissues. Although no cases of scleral invasion or growth into the optic nerve were reported in our study, the 7 T scans were more often (35%) classified as undiagnostic to detect such an invasion, while the majority of the 3 T scans (99%) were found to be of sufficient quality. A side-by-side comparison of similar motion-related artifacts showed furthermore that the localization of these artifacts was generally more intrusive on 7 T scans, explaining part of the observed differences.

### Limitations

One of the main limitations of this study was the lack of DWI in the 7 T protocol. DWI can provide important information for the differential diagnosis of intraocular lesions and is furthermore a potential early predictor of therapy response.<sup>20,22</sup> Due to the magnetic field inhomogeneities in the orbit, the conventionally used EPI read-out does not result in diagnostic images.<sup>16,26</sup> Therefore a single-shot turbo spin echo (TSE) readout was used for ocular DWI at 3 T. Due to the SAR restrictions on 7 T, this sequence is not feasible, and was therefore not included in our protocol.<sup>36</sup> Different approaches have, however, been suggested to enable ocular DWI on 7 T, but these are not yet readily available and were therefore not used in this study.<sup>37,38</sup>

### Conclusions

Overall, UM had similar radiological characteristics on 3 T and 7 T MR images. The evaluated 3 T protocol, however, proved to be superior in assessing the invasion of UM into nearby structures compared to the 7 T scans. Although heterogeneity of small UM was often missed on 3 T, these findings were less clinically relevant which resulted in the 3 T protocol being preferred over the 7 T protocol for clinical evaluations.

### Acknowledgments

Research support was provided by Philips Healthcare. Part of this research was funded by the Dutch Cancer Society (KWF, project number 2019: 12184).

### References

- Singh AD, Turell ME, Topham AK. Uveal melanoma: Trends in incidence, treatment, and survival. *Ophthalmology* 2011;118(9):1881-1885.
- Jager MJ, Shields CL, Cebulla CM, et al. Uveal melanoma. *Nat Rev Dis Primers* 2020;6(1):24.
- Chattopadhyay C, Kim DW, Gombos DS, et al. Uveal melanoma: From diagnosis to treatment and the science in between. *Cancer* 2016;122(15):2299-2312.
- Damato B. Ocular treatment of choroidal melanoma in relation to the prevention of metastatic death – A personal view. *Prog Retin Eye Res* 2018;66:187-199.
- Harbour JW, Onken MD, Roberson ED, et al. Frequent mutation of BAP1 in metastasizing uveal melanomas. *Science* 2010;330(6009):1410-1413.
- Kujala E, Mäkitie T, Kivelä T. Very long-term prognosis of patients with malignant uveal melanoma. *Invest Ophthalmol Vis Sci* 2003;44(11):4651-4659.
- Lane AM, Kim IK, Gragoudas ES. Survival rates in patients after treatment for metastasis from uveal melanoma. *JAMA Ophthalmol* 2018;136(9):981-986.
- Gragoudas ES, Egan KM, Seddon JM, et al. Survival of patients with metastases from uveal melanoma. *Ophthalmology* 1991;98(3):383-389; discussion 90.
- Kaliki S, Shields CL. Uveal melanoma: Relatively rare but deadly cancer. *Eye (Lond)* 2017;31(2):241-257.
- Dogrusöz M, Jager MJ, Damato B. Uveal melanoma treatment and prognostication. *Asia Pac J Ophthalmol (Phila)* 2017;6(2):186-196.
- Rishi P, Koundanya VV, Shields CL. Using risk factors for detection and prognostication of uveal melanoma. *Indian J Ophthalmol* 2015;63(2):110-116.
- Shields CL, Furuta M, Berman EL, et al. Choroidal nevus transformation into melanoma: Analysis of 2514 consecutive cases. *Arch Ophthalmol* 2009;127(8):981-987.
- Ossoinig KC. Standardized echography: Basic principles, clinical applications, and results. *Int Ophthalmol Clin* 1979;19(4):127-210.
- Lemke AJ, Alai-Omid M, Hengst SA, Kazi I, Felix R. Eye imaging with a 3.0-T MRI using a surface coil—A study on volunteers and initial patients with uveal melanoma. *Eur Radiol* 2006;16(5):1084-1089.
- Richdale K, Wassenaar P, Teal Bluestein K, et al. 7 Tesla MR imaging of the human eye in vivo. *J Magn Reson Imaging* 2009;30(5):924-932.
- Niendorf T, Beenakker J-WM, Langner S, et al. Ophthalmic magnetic resonance imaging: Where are we (heading to)? *Curr Eye Res* 2021;46:1-20.
- Grech Fonk L, Ferreira TA, Webb AG, Luyten GPM, Beenakker JM. The economic value of MR-imaging for uveal melanoma. *Clin Ophthalmol* 2020;14:1135-1143.
- Beenakker JW, Ferreira TA, Soemarwoto KP, et al. Clinical evaluation of ultra-high-field MRI for three-dimensional visualisation of tumour size in uveal melanoma patients, with direct relevance to treatment planning. *Magma* 2016;29(3):571-577.
- Fleury E, Trnková P, Erdal E, et al. Three-dimensional MRI-based treatment planning approach for non-invasive ocular proton therapy. *Med Phys* 2021;48(3):1315-1326.
- Kamrava M, Sepahdari AR, Leu K, et al. Quantitative multiparametric MRI in uveal melanoma: Increased tumor permeability may predict monosomy 3. *Neuroradiology* 2015;57(8):833-840.
- Buerk BM, Pulido JS, Chiong I, et al. Vascular perfusion of choroidal melanoma by 3.0 tesla magnetic resonance imaging. *Trans Am Ophthalmol Soc* 2004;102:209-215; discussion 15-7.
- Foti PV, Longo A, Reibaldi M, et al. Uveal melanoma: Quantitative evaluation of diffusion-weighted MR imaging in the response assessment after proton-beam therapy, long-term follow-up. *Radiol Med* 2017;122(2):131-139.
- Beenakker JW, van Rijn GA, Luyten GP, Webb AG. High-resolution MRI of uveal melanoma using a microcoil phased array at 7 T. *NMR Biomed* 2013;26(12):1864-1869.

24. Graessl A, Muhle M, Schwerter M, et al. Ophthalmic magnetic resonance imaging at 7 T using a 6-channel transceiver radiofrequency coil array in healthy subjects and patients with intraocular masses. *Invest Radiol* 2014;49(5):260-270.
25. Lindner T, Langner S, Graessl A, et al. High spatial resolution in vivo magnetic resonance imaging of the human eye, orbit, nervus opticus and optic nerve sheath at 7.0 Tesla. *Exp Eye Res* 2014;125:89-94.
26. Ferreira TA, Grech Fonk L, Jaarsma-Coes MG, van Haren GGR, Marinkovic M, Beenakker JM. MRI of uveal melanoma. *Cancers (Basel)* 2019;11(3):377.
27. Bert RJ, Patz S, Ossiani M, et al. High-resolution MR imaging of the human eye 2005. *Acad Radiol* 2006;13(3):368-378.
28. Bergman L, Nilsson B, Lundell G, Lundell M, Seregard S. Ruthenium brachytherapy for uveal melanoma, 1979-2003: Survival and functional outcomes in the Swedish population. *Ophthalmology* 2005;112(5):834-840.
29. Yuan Y, Kuai XP, Chen XS, Tao XF. Assessment of dynamic contrast-enhanced magnetic resonance imaging in the differentiation of malignant from benign orbital masses. *Eur J Radiol* 2013;82(9):1506-1511.
30. Char DH, Kroll S, Stone RD, Harrie R, Kerman B. Ultrasonographic measurement of uveal melanoma thickness: Interobserver variability. *Br J Ophthalmol* 1990;74(3):183-185.
31. Ferreira TA, Jaarsma-Coes MG, Marinkovic M, Verbist BM, Verdijk R, Jager MJ. Imaging characteristics of uveal melanoma with histopathological validation. *Neuroradiology* 2021. (In press).
32. Steensma BR, Luttje M, Voogt IJ, et al. Comparing signal-to-noise ratio for prostate imaging at 7T and 3T. *J Magn Reson Imaging* 2019;49(5):1446-1455.
33. Maruyama S, Fukunaga M, Fautz H-P, Heidemann R, Sadato N. Comparison of 3T and 7T MRI for the visualization of globus pallidus sub-segments. *Sci Rep* 2019;9(1):18357.
34. Hartevelde AA, van der Kolk AG, van der Worp HB, et al. High-resolution intracranial vessel wall MRI in an elderly asymptomatic population: Comparison of 3T and 7T. *Eur Radiol* 2017;27(4):1585-1595.
35. Ivanov D, Schäfer A, Streicher MN, Heidemann RM, Trampel R, Turner R. A simple low-SAR technique for chemical-shift selection with high-field spin-echo imaging. *Magn Reson Med* 2010;64(2):319-326.
36. Sigmund EE, Gutman D. Diffusion-weighted imaging of the brain at 7 T with echo-planar and turbo spin echo sequences: Preliminary results. *Magn Reson Imaging* 2011;29(6):752-765.
37. Paul K, Graessl A, Rieger J, et al. Diffusion-sensitized ophthalmic magnetic resonance imaging free of geometric distortion at 3.0 and 7.0 T: A feasibility study in healthy subjects and patients with intraocular masses. *Invest Radiol* 2015;50(5):309-321.
38. Paul K, Huelnhagen T, Oberacker E, et al. Multiband diffusion-weighted MRI of the eye and orbit free of geometric distortions using a RARE-EPI hybrid. *NMR Biomed* 2018;31(3):e3872.